



Molecular perspective on starfish tissue extracts: Targeting human carcinoma KB cells for anticancer therapy

Prithviraj Nagarajan^{a,*}, Allur Subramanian Sivakumar^b, Chandramohan Govindasamy^c, Ahmed S. El Newehy^c, Leena Rajathy Port Louis^d, Mohan Sivanandham^e, Kumar Rangarajulu^e, Casimeer C. Sangeetha^f, Ahmad Yousef Ghidan^g, Alaa Yousef Ghidan^h

^a Department of Medical Biotechnology, Aarupadai Veedu Medical College & Hospital, Vinayaka Mission's Research Foundation (Deemed to be University), Kirumampakkam, Puducherry 607402, India

^b Department of Orthopaedic Surgery, Dongtan Sacred Heart Hospital, Hallym University, College of Medicine, Hwaseong 18450, Republic of Korea

^c Department of Community Health Sciences, College of Applied Medical Sciences, King Saud University, P.O. Box 10219, Riyadh 11433, Saudi Arabia

^d Department of Pharmacology, Aarupadai Veedu Medical College & Hospital, Vinayaka Mission's Research Foundation (Deemed to be University), Kirumampakkam, Puducherry 607402, India

^e Department of Biochemistry, Aarupadai Veedu Medical College & Hospital, Vinayaka Mission's Research Foundation (Deemed to be University), Kirumampakkam, Puducherry 607402, India

^f Department of Physics, Sri Padmavati Mahila Visvavidyalayam (Women University), Andhra Pradesh 517502, India

^g Department of Anesthesiology and Pain Medicine, Mount Sinai Hospital, University of Toronto, Toronto, Ontario M5G 1X5, Canada

^h Nanotechnology and Microbiology, Research and Development Center, The Higher Council for Science and Technology, Amman, 11941, Jordan

ARTICLE INFO

Keywords:

Bioactive
Anticancer
Cytotoxicity
Apoptosis
Antioxidant
Regeneration tissue extracts

ABSTRACT

The marine environment is rich in natural bioactive compounds, including zebrafish and starfish species, which have garnered attention in drug research for their remarkable tissue regeneration abilities. Zebrafish, in particular, share a genetic resemblance of around 70% with humans. We chose to investigate *Luidia maculata*, a starfish species, due to its remarkable tissue regeneration abilities and the potential bioactive compounds it holds, making it a promising candidate for anticancer and antioxidant therapies. Human KB carcinoma cells were subjected to *L. maculata* tissue extracts to assess cytotoxicity using the MTT test. Intracellular ROS levels were measured via DCFH-DA, and mitochondrial membrane potential changes were evaluated using Rh-123 staining. Oxidative DNA damage was examined with the comet test, while morphological apoptotic changes were observed through the AO/EtBr dual staining technique. The active compounds in the starfish extracts were identified using HPLC, GC-MS/MS, and FTIR analyses. The bioactive fractions extracted from *L. maculata* demonstrated significant anti-proliferative effects on KB carcinoma cells, inducing apoptosis. These fractions led to a notable increase in intracellular ROS levels, resulting in alterations in mitochondrial membrane potential and oxidative DNA damage in the cells. Upregulation of Bax/Caspase 3 protein expression and downregulation of Bcl-2 protein expression indicated the involvement of apoptotic pathways. Comprehensive analyses confirmed 35 starfish-derived anticancer compounds that inhibit cell proliferation, induce apoptosis, and target cancer-related pathways. Additionally, our study underscores the antioxidant potential of *L. maculata* starfish extracts, offering insights into marine organism-based therapies with promising medical applications.

1. Introduction

Echinoderms, especially starfish, possess remarkable natural regenerative abilities, attracting significant attention from researchers and

pharmacologists worldwide. Their exceptional regenerative skills serve diverse biological purposes and have garnered interest for potential therapeutic applications (Ben Khadra et al., 2018). Certain starfish species, such as *Luidia senegalensis*, *Oreaster reticulatus*, and *Echinaster*

Peer review under responsibility of King Saud University and Aarupadai Veedu Medical College & Hospital, Vinayaka Mission's Research Foundation (Deemed to be University), Kirumampakkam, Puducherry- 607402

* Corresponding author.

E-mail address: prithivinaga@gmail.com (P. Nagarajan).

<https://doi.org/10.1016/j.jksus.2023.103035>

Received 27 August 2023; Received in revised form 15 November 2023; Accepted 26 November 2023

Available online 27 November 2023

1018-3647/© 2023 The Authors. Published by Elsevier B.V. on behalf of King Saud University. This is an open access article under the CC BY-NC-ND license (<http://creativecommons.org/licenses/by-nc-nd/4.0/>).

sp., have traditionally been used in Brazilian countries for treating conditions like bronchial asthma, hypertension, diabetes, and cardiac diseases (Meyer-Rochow, 2017). Starfish extracts have been found to contain numerous biologically active compounds, including cerebroside, glycosides, glycosyl ceramides, steroids, astrosaponin, anthraquinones, peptides, monosaccharides, and polysaccharides, exhibiting various pharmacological properties, such as hemolytic, cytotoxic, antiviral, antifungal, anti-asthmatic, antimutagenic, analgesic, and antimicrobial effects. Consequently, there is a need to screen and analyze metabolites from *L. maculata*, a species of starfish (Dong et al., 2011).

Antioxidants are crucial in combating oxidative damage and enhancing the immune system against cancer and degenerative diseases (Venkatachalam et al., 2018). Marine protein hydrolysates derived from various sources, such as fish, squid, conger eel, jellyfish, microalgae, and green mussels, have demonstrated potential antioxidant properties (Balamurugan et al., 2017). While terrestrial plant products have been extensively studied for their pharmacological and biological properties, research on echinoderm extracts with antioxidant properties remains limited. The regenerated biomaterials from *L. maculata* starfish have yet to be thoroughly characterized. Organisms maintain ROS (reactive oxygen species) homeostasis through mitochondrial apoptosis, wherein apoptotic signaling pathways are inhibited, and the mitochondrial membrane depolarizes, resulting in increased levels of pro-apoptotic molecules in the cytosol. The induction of apoptosis is crucial for inhibiting cancer cell growth (Mann, 2002).

Numerous extraction techniques have been developed to isolate novel secondary metabolites from aquatic organisms, including sponges, seaweed, algae, and other marine invertebrates, which are potential sources of therapeutics for human diseases, including cancer (Verissimo et al., 2021). Echinoderms, including sea cucumbers, urchins, and starfish, have been particularly interesting due to their regenerative abilities and compounds with potential chemotherapeutic effects and apoptotic changes in cancer cell lines (García-Arrarás and Dolmatov, 2010). Previous studies have investigated the pharmacological properties of crude extracts of *Luidia maculata* (*L. maculata*). However, the bioactive compounds with antioxidant and anticancer effects from *L. maculata* regenerated tissue extracts still need to be identified, characterized and studied for their biological properties. Notably, no publication has reported the partial purification of a bioassay-guided fractionation from an amputated starfish. Our research unfolds a multifaceted mission as we investigate the anticancer properties of *L. maculata* starfish tissue extracts on KB carcinoma cells. Beyond our overarching goal, we aimed to assess the innate antioxidant and anticancer potential in *L. maculata* regenerated tissue extracts. Simultaneously, we endeavor to decipher the intricate mechanisms underlying their actions on KB cancer cell lines. We meticulously identify their hydrophobic constituents by employing state-of-the-art GC/MS/MS techniques. This comprehensive study aims to deepen our comprehension of the biological properties of starfish regeneration extracts and specifically emphasizes unravelling their anticancer mechanisms. By embracing these diverse objectives, our research aspires to reveal the multifaceted dimensions of starfish regeneration extracts and their promising role in combating cancer while fostering wound healing.

2. Materials and methods

2.1. Ethics declaration

In adherence to Indian ethics regulations, all animal experiments involving *L. maculata* were conducted, considering this species is neither endangered nor protected. The specimens were thoughtfully released into their natural habitat after completing the experimental procedures.

2.2. Animal regeneration experiments

Specimens of *L. maculata* (diameter 10–15 cm) were collected at a

depth range of 10 to 15 m from Rameswaram Island in the Indian Ocean with the assistance of scuba divers (Fig. S1a-b). Starfish with no previous symptoms of regeneration were collected and kept at 15 °C in aquaria with seawater throughout the experimental duration. The starfish were fed small pieces of blue mussels (*Mytilus edulis*) twice a week. To induce regeneration, the starfish were anaesthetized with 4 % magnesium chloride in 50 % artificial seawater, and approximately 0.5 cm of the distal third of three arms for each specimen was amputated using a scalpel. The specimens were allowed to regenerate in the aquarium. The laboratory animal care committee of Aarupadai Medical College and Hospital, Puducherry, India, approved the experimental methods.

2.3. Preparation, purification, and fractionation of starfish extract

The extraction scheme for bioassay-guided fractionation from amputated *L. maculata* extracts using different solvents is shown in Fig. S2. Briefly, three-arm tips of each starfish specimen were amputated approximately 1.5 cm in length. The entire amputated starfish arm was macerated for 24 h at room temperature and refluxed in 6L of 70 % ethanol for 60 min (2.5 kg). Active fractions were pooled and condensed at 40 °C using a rotary evaporator, yielding 140 g of crude extract (LM-CE). The glassy brown suspension was dissolved in water and extracted three times with an equivalent amount of ether (petroleum) to obtain non-polar fraction compounds, such as lipids. The defatted water process was divided into ethyl acetate (EtOAc) and n-butanol (BuOH) fractions, yielding the ethyl acetate-derived portion (LM-EA-E, 49 g), the n-butanol fraction (LM-nB-E, 38 g), and the water-soluble fraction (LM-WS-E, 54 g). Furthermore, LM-nB-E was further fractionated using a chromatography column of Diaion HP-20 with H₂O-MeOH solvent (100:0, 80:20, 70:30, 60:40, 40:60, 30:70, 20:80, 10:90, 0:100) to yield ten acetone fractions (LM-nB-E-Fr.1–10). The fraction eluted with H₂O/MeOH (10:90) (LM-nB-E-Fr8) was further fractionated using a preparative C18 HPLC column with 80 % aqueous methanol and flow rates of 1 ml/min to obtain five active fractions. The optimization of this preparative C18 HPLC column separation involved adjustments in solvent composition, flow rate, and gradient conditions. The goal was to efficiently elute five active fractions representing distinct bioactive compounds for subsequent analysis and experimental investigations. Active fractions representing each peak were eluted and pooled together from HPLC (LM-nB-E-Fr8.1–5, 1.35 g) as a white amorphous powder (hereafter referred to as the bioactive fraction), which was analyzed for GC-MS/MS study. The isolated fractions were dissolved at 100 mg/ml concentrations in 10 % dimethyl sulfoxide (DMSO) for further experimental investigations.

2.4. Identification of the purified compounds

The active peak fraction collected from the HPLC was pooled and further analyzed to identify pharmacologically active constituents using the A7890 GC fuel chromatography MS (GC-MS) system. A quadrupole MS 5975C detector (30 m long, internal 0.25-mm diameter, 0.25 µm thickness; Agilent technology, Germany) with helium as a carrier gas was used to quantify the detected compounds. The injector size and temperature were 2 µl and 250 °C, respectively. The samples were injected into the column after 1 min at 50 °C and then heated at a rate of 25°C/min to 170°C and 5°C/min to 280°C, respectively. The spectra were scanned in the 33–600 *m/z* range. The MS was run in electron ionization mode, and the collected mass spectra were compared to the MS software used in the NIST library databases.

2.5. In vitro screening of crude extracts and active fractions

Human oral epidermoid carcinoma KB cells were cultivated in RPMI1640 medium supplemented with 10 % fetal bovine serum and 1 % glutamine and incubated at 37 °C with 5 % CO₂. The KB cells were seeded at a density of 1 × 10⁶ cells per well in 96-well plates and

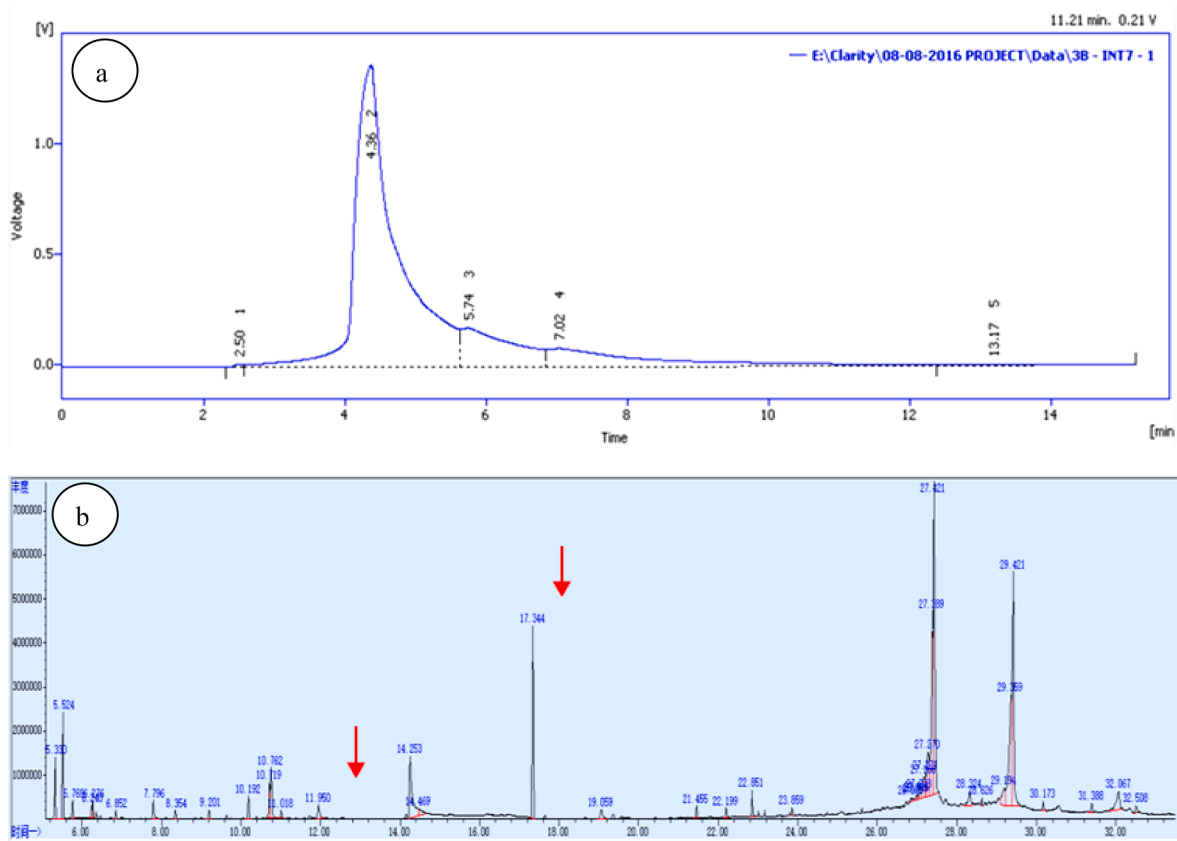


Fig. 1. HPLC a) and GC-MS/MS b) chromatogram of the bioactive fraction of *L. maculata*.

incubated for 24 h. Cells were treated with crude extracts and active fractions at different concentrations of *L. maculata* tissue extracts, ranging from 0.1 $\mu\text{g/ml}$ to 10 $\mu\text{g/ml}$ for 24 h, and DMSO was used as a control. After achieving 90 % confluence, attached cells were washed twice with phosphate buffer solution, and 20 μl of MTT solution was added to each well. After overnight incubation at 37 $^{\circ}\text{C}$, the MTT solution was removed, and DMSO was added to dissolve the formazan crystals produced by viable cells. Plates were agitated for 10 min, and absorbance was measured at 570 nm using a microplate reader. Cell viability was determined by comparing the absorbance of samples treated with cells to the absorbance of control cells. The IC_{50} value was calculated using linear regression analysis and repeated in triplicate for each concentration.

2.6. Cell migration assay

An in vitro cell wound healing assay was performed to study the migratory behavior of KB cells. Confluent KB cell monolayers (approximately 90 %) were manually wounded by scratching the cells with a sterile P200 pipette tip. Following the manual scratching, there was an incubation period of 24 h to allow the cells to respond and migrate. The wounded cells were cultured in a new medium containing *L. maculata* active fractions (1 $\mu\text{g/ml}$), crude, and controlled after washing the cellular debris twice with PBS. Healing of wounds was captured using an Olympus optical camera with a light microscope, and direct measurements of repaired regions were documented to measure cell migration (Mariadoss et al., 2021).

2.7. DPPH radical scavenging assay

The extract scavenging activity was assessed using the DPPH assay (Zhu et al., 2011). 1.5 ml of DPPH solution (0.1 mM methanolic

solution) was mixed with 1 ml of the sample at various concentrations. The reaction mixture was stirred for 30 min in the dark and then absorbed by a spectrophotometer at 517 nm. A control group with 0.1 ml (10 mg/ml) of ascorbic acid was used. The DPPH radical scavenging percentage was calculated using the following formula:

$$(\% \text{Inhibition}) = \frac{(\text{Absorbance of control} - \text{Absorbance of sample})}{\text{Absorbance of control}} \times 100$$

2.8. ABTS⁺ radical scavenging activity

The radical scavenging activity of ABTS + was measured according to the procedures (Ilyasov et al., 2020). The ABTS⁺ solution was prepared and stored at room temperature for 16 h. Then, 1 ml of the ABTS + solution was mixed with 30 ml of deionized water to obtain a workable solution of 0.02 ± 0.70 at 734 nm. To 150 μl of the work solution, 1 ml of samples at various levels was added, and the reaction mixture was kept in a dark room for about 10 min before measuring absorbance at 734 nm. A standard control with 0.1 ml of ascorbic acid (10 mg/ml) was used. The ABTS scavenging activity was calculated using the following formula:

$$(\% \text{Inhibition}) = \frac{(\text{Absorbance of control} - \text{Absorbance of sample})}{\text{Absorbance of control}} \times 100$$

2.9. Superoxide radical scavenging activity

The superoxide radical scavenging activity of samples was determined according to the procedures (Zhu et al., 2006). The reaction mixture consisted of 150 μM nitro tetrazolium, 1 ml of aliquots (prepared in 0.1 M Tris HCL buffer, pH 7.4 of 60 μM phenazine methosulphate), and 468 μM nicotinamide adenine dinucleotide added to 1 ml of the sample at varying concentrations. The reaction mixture was then

incubated for 5 min at 25 °C, and absorbance was measured at 560 nm. A standard control with 0.1 ml of ascorbic acid (10 mg/ml) was used. The superoxide radical scavenging activity was calculated using the following formula:

$$(\%Inhibition) = \frac{(Absorbance\ of\ control - Absorbance\ of\ sample)}{Absorbance\ of\ control} \times 100$$

2.10. Hydrogen peroxide radical scavenging activity

The hydrogen peroxide scavenging activity of the samples was determined according to the method of (Gülçin et al., 2004). A 40 mM hydrogen peroxide solution was prepared in PBS, and 1 ml of extracts was mixed gently with 2 ml of 40 mM hydrogen peroxide solution. The sample absorbance reaction mixtures were measured at 230 nm, this specific wavelength, chosen for its characteristic absorption peak related to hydrogen peroxide, enables us to assess the ability of the sample to neutralize this reactive oxygen species (ROS). Hydrogen peroxide is an important ROS involved in oxidative stress and cellular damage, rendering it a relevant target for antioxidant assessment. A standard control with 0.1 ml ascorbic acid (10 mg/ml) was used. The hydrogen peroxide scavenging activity was calculated using the following formula:

$$(\%Inhibition) = \frac{(Absorbance\ of\ control - Absorbance\ of\ sample)}{Absorbance\ of\ control} \times 100$$

2.11. HPLC: Amino acid composition analysis

The active fraction's amino acid composition was determined by the HPLC method (Merck Hitachi Lachrome D-7000 HPLC System) using a Shimadzu C-18 column connected with two solvent systems: (a) 0.1 % TFA solutions and (b) 0.1 % TFA in 90 % acetonitrile (Baker and Han, 1994). The samples were hydrolyzed in 6 M HCL for 24 h in vacuum-sealed ampoules at 110 °C, and then hydrolysates were analyzed on a Hitachi liquid chromatography system at room temperature. The HPLC system was used to identify and quantify amino acids by comparing retention time and peak areas to those of a standard amino acid composition (Sigma). The absorbance of HPLC column elutes was measured at 280 nm.

2.12. GC-MS: Fatty acid profile analysis

The fatty acid compositions of the active fraction extract were determined by GC-MS using a Varian Saturn 2000R gas chromatograph (Hewlett Packard 5890 model) programmed from 50 °C to 225 °C (40 °C/min), then kept constant for 30 min. FAMES were categorized based on their electron effects MS spectra and retention time (Rt), which were comparable to a standard (Sigma), and quantified based on relative peak areas (Bligh and Dyer, 1959).

2.13. FT-IR (Fourier transformed infrared) spectroscopy

The FT-IR spectrometer (Thermo Nicolet, USA) was used to quantify the functional properties of the samples (Mariadoss et al., 2019a). Diffuse reflectance was applied in the mid-IR spectral region (400–4000 cm⁻¹). The extracted sample (2 mg) was compressed into a salt disc using a compression gauge (10 mm diameter) by combining it with 100 mg of potassium drying bromide powder (KBr). ORIGIN 8.0 software was used to investigate the peak absorption of light intensity.

2.14. Measurement of intracellular ROS levels in cells

The oxidation level of 2,7-diacetyl dichlorofluorescein (DCFH-DH; Sigma-Aldrich) was measured to determine the intracellular reactive

oxygen (ROS) concentration, as described by (Sivaraj et al., 2018). The cells were seeded at a density of 5 × 10⁴ cells/well into dark 96-well tissue culture plates and treated for 3 h with 1 µg/ml of crude and active fractions. Then, the cells were stained for 30 min at 37 °C in the dark with 10 M DCFH-DA and rinsed with PBS thrice. Images were photographed using a fluorescence microscope (Nikon, Japan) at a magnification of 400. Using a microplate reader, Fluorescence was measured at excitation and emission wavelengths of 485 and 335 nm, respectively.

2.15. Morphological evaluation of apoptotic cells by acridine orange and ethidium bromide (AO/EtBr)

The AO/EtBr double staining test examined the apoptosis-related morphological alterations (Qingming et al., 2010). In a 24-well plate, 2 × 10⁵ cells were plated in each well and incubated for 24 h before being treated with crude and active fractions for another 24 h at 37 °C. The cells were washed twice with 1 × PBS and stained with 5 µl of AO/EB. Finally, fluorescent microscopy (Olympus) examined the cell morphology at 20 × magnification. Apoptotic cells were distinguished by morphological characteristics such as constricted cell bodies, condensed, consistently delimited, heavily coloured chromatin, and membrane-bound apoptotic bodies.

2.16. DNA damage analysis

DNA fragmentation, indicative of apoptosis, was assessed through alkaline single-cell gel electrophoresis, commonly called the comet assay, as described by (Gunaseelan et al., 2017). In this assay, cells were embedded in agarose gel on microscope slides, electrophoresed under alkaline conditions, and stained with a fluorescent DNA-binding dye. Subsequently, comet photographs were captured using an epifluorescence microscope (Nikon, Japan). The movement of the DNA tail and its length damage were calculated using CASP software. The images were used to measure individual nuclei's DNA content and calculate the percentage of DNA loss in the comet tail.

2.17. Western blot analysis

The cells (1 × 10⁶ cells/well) were treated with 1 µg/mL of control, crude, and active fractions. Samples were washed with PBS lysis buffer and centrifuged at 12,000 × g for 15 min. The NanoDrop was used to measure the protein concentrations of the samples. Aliquots of the lysates (30 µg of protein) were boiled for 5 min at 95 °C and transferred onto nitrocellulose membranes for blotting. Primary antibodies Bax (B3428) (Sigma), Bcl-2 (B9804) (Sigma), Caspase-3 (C5737) (Sigma), PCNA (SAB4100556) (Sigma), Cyclin-D1 (C7464) (Sigma), and β-actin (A2228) (Sigma) were used to probe the membranes for 1 h in TTBS. After that, the membranes were rinsed three times with TTBS at 10-minute intervals before being incubated with secondary antibodies immunoglobulin-G-horseradish peroxidase for two hours at 37 °C. Chemiluminescence was used to detect the protein bands, which were then visualized using the luminescent image Studio device (LI-COR).

2.18. Statistical analysis

Statistical analysis of the results was performed using Version 5.0 of GraphPad Prism. Samples were collected in triplicate for each experiment, and one-way analysis of variance (ANOVA) was used to assess the variations between the control and active fractions. ANOVA analysis was used to compare the data from various samplings to evaluate the variations between the control and fraction.

3. Results

3.1. HPLC evaluation of *L. maculata* active fractions

The HPLC chromatograms of *L. maculata* are displayed in Fig. 1a. The partially purified fraction observed five peaks with retention times of 2.50, 4.36, 5.74, 7.02, and 13.17 min. The presence of the active compound in the fractions was indicated by the most prominent and broadest peak at 4.36 min, while peaks at 5.74 and 7.02 min suggested the presence of other biologically active compounds. These retention times serve as key indicators of the compounds presence and are vital for the identification and characterization of bioactive components in *L. maculata* tissue extracts.

3.2. Analysis of GC-MS/MS

To confirm the presence of the compounds in the bioactive fraction, we performed an analysis, as shown in Fig. 1B and detailed in Table S1. In this analysis, we identified compounds such as 5-cholest-7-en-3-ol, hexadecanoic acid, myo-inositol, 9,12,15-Octadecatrienoic acid, and 9,12-Octadecadienoic acid within the active fraction. Importantly, these compounds have demonstrated anticancer activity in various cell lines, including KB. While our study primarily focused on their identification and biological activities, the specific biosynthetic pathways responsible for these compounds within *L. maculata* were not investigated in detail

in this study. We further verified these bioactive compounds' identities and biological activities using Dr. Dukes' phytochemical and elucidation techniques (Duke and Bogenschutz, 1994). This comprehensive approach confirmed their presence and established their specific chemical identity and ability to exhibit anticancer effects on KB cell lines. Our combined analytical and biological validation ensures the reliability of our findings and supports the bioactive nature of these compounds in the active fraction of *L. maculata* extract.

3.3. Cell proliferation and anti-migration effects induced by *L. maculata* bioactive fraction

The effect of the *L. maculata* bioactive fraction on cell growth and proliferation was assessed using the MTT assay. Fig. 2a illustrates a significant inhibition of KB cell proliferation by the active fraction after a 24-hour incubation period compared to the control and crude groups. Concentrations of 25, 50, or 100 $\mu\text{g/ml}$ of the extracts did not significantly affect *L. maculata*. A dose-dependent response was observed with the active fractions effectively inhibiting KB cell growth at concentrations of 0.3, 0.78, 1.56, 3.12, and 6.25 $\mu\text{g/ml}$. The IC₅₀ value of cell growth was determined to be 0.62 $\mu\text{g/ml}$, indicating a potent anti-proliferative effect of the active fraction. Moreover, treatments with active fractions at 6.25 $\mu\text{g/ml}$ and 12.5 $\mu\text{g/ml}$ demonstrated approximately 80 to 81 % inhibition of cell proliferation, respectively.

Apoptotic morphological changes were also observed, including

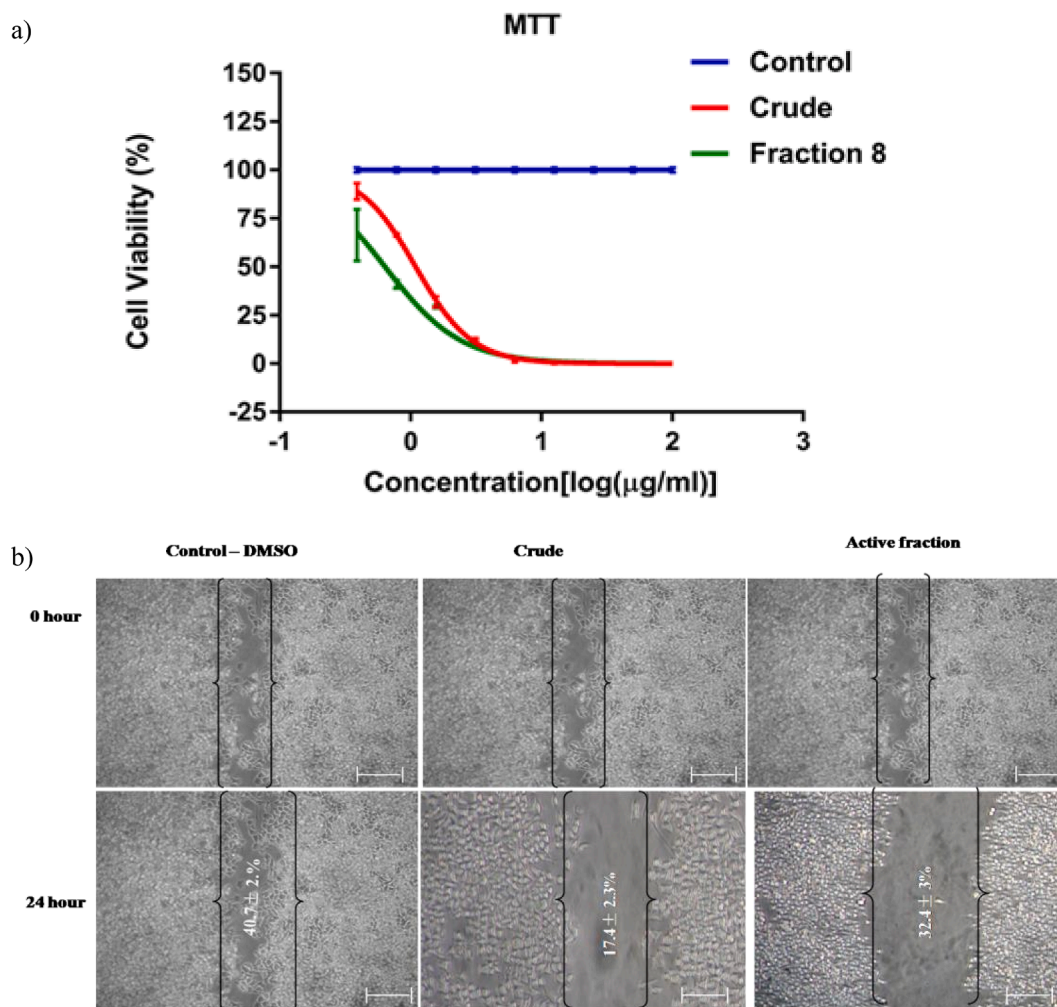


Fig. 2. The cytotoxicity assay shows the impact of *L. maculata* active fraction on KB cells (a). The wound healing test was conducted on KB cells treated with 1 $\mu\text{g/ml}$ control, crud, and active fractions for 24 h (b). T-Scratch software was used to capture and analyze wound edge photographs of cells treated with individual triplicates 24 h after treatment, allowing calculation of the percentage of migration.

nuclear chromatin attention, edge accumulation, cytoplasmic hyper-vacuolization, cellular shrinkage, and apoptotic bodies. Based on the MTT effects, working concentrations for further experiments were determined to be 0.3, 0.78, 1.56, and 3.12 $\mu\text{g/ml}$ for active fractions. Furthermore, the potential impact of active fractions and crude extracts on KB cell migration was observed (Fig. 2b). The MTT assay confirmed that cells treated with active fractions migrated slower than untreated and crude extract-treated cells. Morphologically, the KB cells treated with the active fraction exhibited reduced adhesion, resulting in cell shrinkage and the appearance of apoptotic bodies. They eventually merged into massive cellular aggregates. In contrast, no distinct phenotypes or directional migrations were observed in cells treated with untreated and crude extracts. These results indicate that active fractions of *L. maculata* are crucial in regulating cell proliferation and behavior.

3.4. Evaluation of antioxidant activities by *L. maculata* bioactive fraction

The scavenging of DPPH radicals by the extracts significantly increased DPPH concentrations (Fig. 3a). The most substantial DPPH radical scavenging activities were observed in the active fractions, control, and crude extracts, indicating a higher concentration of potent antioxidants than the crude and control samples. Similarly, the ABTS⁺ radical scavenging activity aligned with the DPPH results, with the active fraction exhibiting the highest ABTS⁺ radical activity, followed by the dose-dependent control and crude activities (Fig. 3b). The study also evaluated the radical scavenging activity of the three different extracts in KB cells, considering that most cancer cell lines produce superoxide radicals, leading to oxidative stress and cellular damage (Fig. 3c). The active fraction displayed the highest scavenging activity of 80 % at 30 $\mu\text{g/ml}$ and the lowest activity of 20 % at 5 $\mu\text{g/ml}$, demonstrating superior superoxide (O_2^-) radical scavenging activities compared to the control and crude extracts.

Finally, the study assessed the hydroxyl radical scavenging activity,

crucial for preventing cellular damage caused by reactive hydroxyl radicals (Fig. 3d). The crude extract exhibited the highest hydroxyl radical scavenging activity, followed by the active fraction and the control. The findings regarding antioxidant activities highlight the robust scavenging potential of the active fraction of *L. maculata* against various free radicals. This potent antioxidant capacity contributes to its potential therapeutic efficacy as an efficient antioxidant agent.

3.5. Amino acid composition analysis of *L. maculata* active fraction

The amino acid composition of the active fraction was determined by conducting an HPLC analysis, comparing it with 21 amino acid standards (Fig. 4a). The active fraction exhibited enrichment in essential amino acids (EAAs) such as Histidine, followed by Phenylalanine, Methionine, Valine, Lysine, Tryptophan, Isoleucine, and Leucine. Conversely, non-essential amino acids (NEAAs) like asparagine, Alanine, Glycine, Aspartic acid, Glutamine, Glutamic acid, Proline, Tyrosine, and Serine were present in lower quantities in the active fraction (Fig. 4b, Table 1). HPLC analysis facilitated identifying and quantifying specific amino acids in the active fraction of *L. maculata*. The higher proportions of essential amino acids imply that the active fraction holds significant nutritional and therapeutic potential, warranting further scientific investigation.

3.6. Fatty acid composition analysis of *L. maculata* active fraction

The fatty acid composition of the active fraction was determined using gas chromatography FAME. Polyunsaturated fatty acids (PUFAs) were more abundant in the active fraction than saturated fatty acids. The primary components identified among the PUFAs were α -Linoleic acid C18:3 (545.6 mg) and Linoleic acid C18:2 (306.2 mg). Additionally, Oleic acid C18:1 (112.6 mg) was identified as the dominant mono-unsaturated fatty acid (MUFA) based on the standard's Rf value (Fig. 4c-

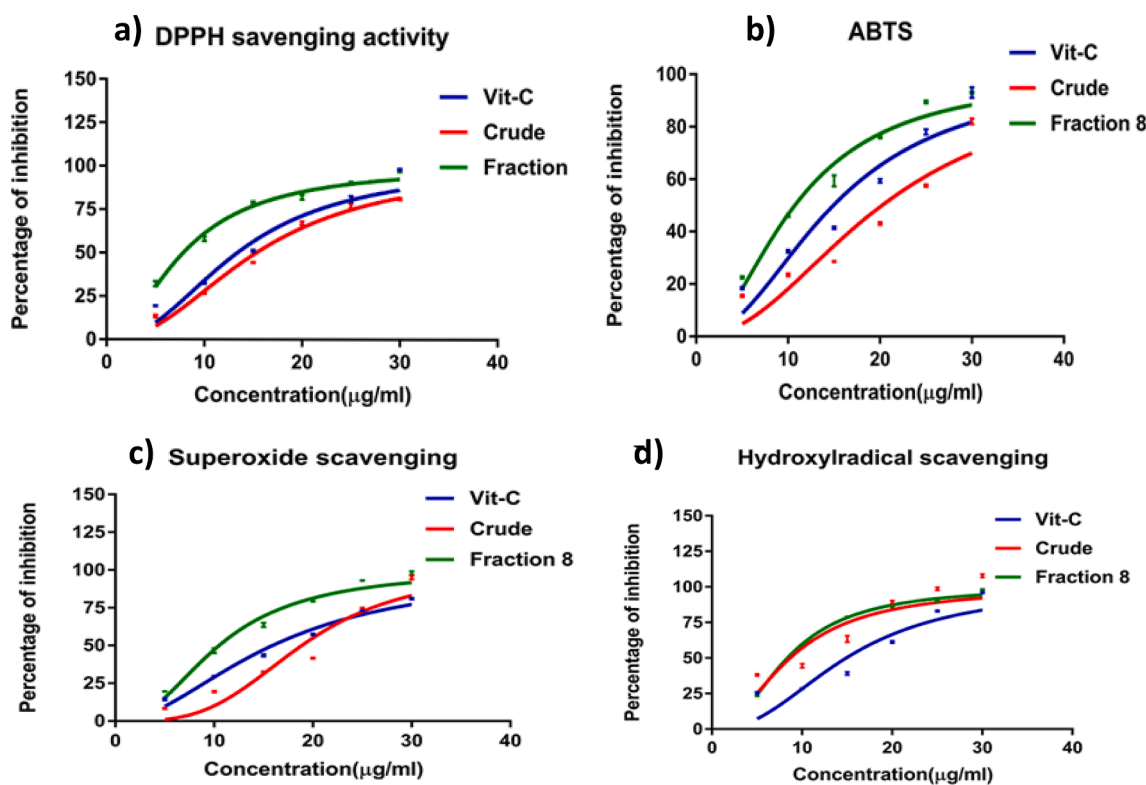


Fig. 3. The antioxidant activities were assessed through DPPH radical scavenging (a), ABTS radical scavenging (b), superoxide radical scavenging (c), and hydroxyl radical scavenging activity (d). The results are presented as the mean \pm standard deviation of six experiments from each sample, with values significantly different ($P < 0.05$) from the control values.

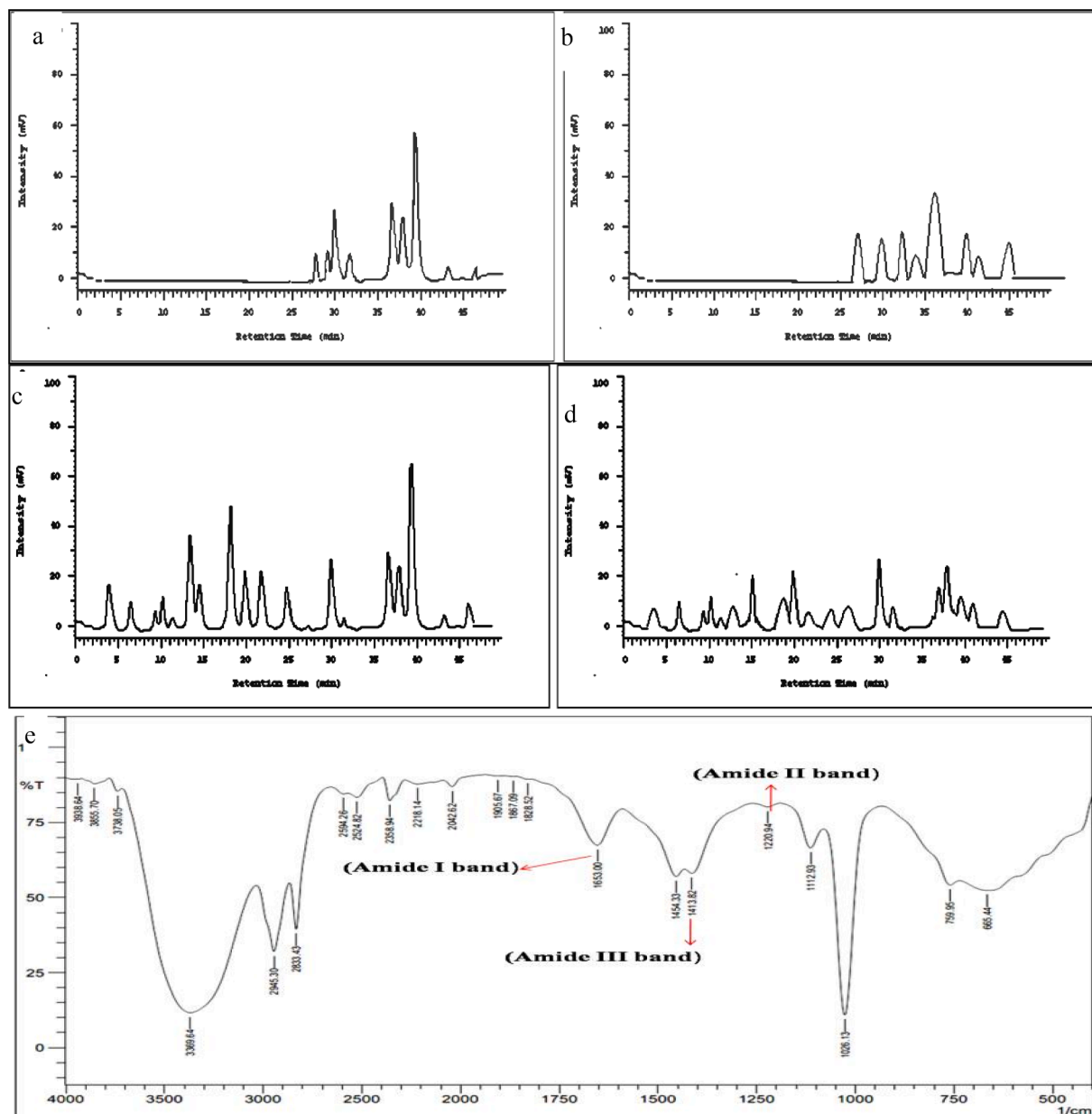


Fig. 4. Standard Amino Acid Graph (a). Amino Acid Content of the Active Fraction (b), Gas Chromatography FAME: Profiling Fatty Acid Composition (c). Fatty Acid Content of the Active Fraction: The gas chromatography analysis identified fatty acid components in *L. maculata* active fraction, showing richness in PUFAs and significant SFAs (d). The Characteristic peaks corresponding to various functional groups were observed in the FT-IR Analysis of *L. maculata* Active Fraction, suggesting the presence of diverse compounds, including hydrophobic components, in the active fraction (e).

d and Table 2). In addition to PUFAs and MUFAs, significant amounts of saturated fatty acids (SFAs) were present in the active fraction. Notably, Stearic acid C18:0 (325.70 mg), Margoric acid C17:0 (103.3 mg), and Palmitic acid C16:0 (34.7 mg) were identified as the most important components of SFAs. The predominance of PUFAs and MUFAs in the active fraction suggests potential health benefits and functional properties, warranting further research in nutrition and health sciences.

3.7. FTIR characterization of the active fraction

The active fraction was subjected to FTIR evaluation to characterize its functional groups (Fig. 4e and Table 3) and compare them with standard FTIR data (Krimm and Bandekar, 1986). Free anti-symmetry O–H hydrogen-bonded stretching frequencies were indicated by a strong and sharp peak between 3738.64 cm^{-1} and 3938.64 cm^{-1} . Moreover, amides and primary amine groups with N–H stretching

frequency at 3369.64 cm^{-1} and nitrile compounds with N–O asymmetric deformation at 2358.94 cm^{-1} were identified in the active fraction. Additionally, C–H stretching vibrations of free sugars, a saturated aliphatic CO_2 stretching band between 1828.52 cm^{-1} and 1905.67 cm^{-1} , and an aliphatic CH_2 stretching band at 1454 cm^{-1} with aliphatic-CH bending frequency were observed in the active fraction, pointing to the presence of hydrophobic compounds. Furthermore, the observation of alkene groups at 1653 cm^{-1} indicated the existence of low C–C ring stretching frequency. The presence of hydrophobic compounds in the active fraction was further supported by the fingerprint range of carbohydrates, which was positioned between 665 and 1220 cm^{-1} (Al-Assaf et al., 2007).

3.8. Intracellular ROS induction by *L. maculata* active fraction

Intracellular reactive oxygen species (ROS) accumulation is a

Table 1
The amino acid content of active fraction.

No	Essential amino acids (EAA)	Concentrations (mg/ 100 g)	Non-essential amino acids (NEAA)	Concentrations (mg/ 100 g)
1	Histidine	5257.3	Asparagine	5354.7
2	Phenylalanine	3254.6	Alanine	4135.7
3	Methionine	3103.6	Glycine	3908.6
4	Valine	2905.4	Aspartic Acid	3556.7
5	Lysine	1093.4	Glutamine	3356.8
6	Tryptophan	904.3	Glutamic Acid	3305.8
7	Iso-Leucine	456.7	Proline	3256.7
8	Leucine	233.6	Tyrosine	2984.6
9			Serine	2904.5
	Total (EAA)	17208.9	Total (NEAA)	32764.1

Table 2
The fatty acids content of active fraction.

Composition of fatty acids	Carbon nomenclature	Retention time	Area %	Concentrations (mg/ 100 g)
Saturated fatty acids (SFA)				
Stearic acid	C 18:0	33.5	10.4	325.7
Margaric acid	C 17:0	30.8	12.32	103.3
Palmitic acid	C 16:0	30.6	16.75	34.7
	Total saturated fatty acids			463.6
Monosaturated fatty acids (MUFA)				
Oleic acid	C 18:1	35.5	26.28	112.6
	Total monosaturated fatty acids			112.6
Polysaturated fatty acids (PUFA)				
Alpha linolenic acid	C18:3	40.2	10.74	545.6
Linolenic acid	C18:2	37.2	11.38	306.2
Moroctic acid	C18:4	44.6	24.45	93.2
Docosahexaenoic acid	C22:6	45.4	8.238	81.6
Eicosapentaenoic acid	C20:5	46.3	7.72	55.3
	Total polyunsaturated fatty acids		1081.9	

Table 3
FT-IR analysis of *L. maculata* active fraction.

Wavelength range (cm ⁻¹)	Assignment	Functional groups
665.44	C-BR stretch	Alkyl halides
759.95	C-Stretch	Alkyl halide
1026–1220.94	C-N stretch	Aliphatic Amines
1220.94	N–H in plane bending/C-N stretching vibration	Amide II bands (Secondary amines group)
1413.82	C-N stretching vibration	Amide III bands (C-N Primary amines)
1454.33	CH ₂ stretch vibration	CH 2aliphatic compounds
1653	C = O stretching vibration	Amide I bands (Primary amines)
1828.52–1905.67	C = O stretch	Saturated aliphatic, Esters
2042.62–2218.14	H-C = O:C-stretch	Aldehydes
2358.94	C = stretch	Nitriles
2524.82–2594.26	H-C = O:C-H stretch	Aldehydes
2833.43–2945.30	C-H stretch	Alkanes
3369.64	N–H stretch	Amides and primary Arimes
3738.64–3938.64	O–H stretch, free	Alcohols (strong and sharp)

hallmark of the apoptotic process. Following the treatment of KB cells with control, crude, and active fractions, a significant elevation in ROS levels was observed, with the active fraction demonstrating the most substantial ROS generation (95 %), as depicted in Fig. 5a-b. These findings suggest that the induction of apoptosis may be attributed to the

generation of ROS by the active materials present in *L. maculata*.

3.9. Apoptotic morphological changes in cancer KB cells induced by the active fraction of *L. maculata*

To elaborate on the mechanisms by which *L. maculata* extracts induce apoptosis in KB carcinoma cells, our study employed multiple approaches. First, we assessed apoptotic morphological changes using acridine orange/ethidium bromide (AO/EB) double staining. Additionally, intracellular ROS accumulation was monitored (Fig. 5c). When not treated with the active fraction, the cancer KB cells displayed red/orange (EtBr stained) and green (AO stained) fluorescence. In contrast, when exposed to the active fraction, the cells exhibited typical apoptotic features, including cellular shrinkage, chromatin condensation, nuclear fragmentation, and the formation of apoptotic bodies. Remarkably, even at a concentration as low as 1 µg/ml, the active fraction induced apoptosis in 80 percent of the cells, showcasing its superior efficacy compared to other extracts. These observations strongly support the mechanisms by which *L. maculata* extract induces apoptosis in KB carcinoma cells highlighting the potential of the active fraction as a potent agent in combating cancer cells.

3.10. Induction of DNA damage by the active fraction of *L. maculata*: A comet assay analysis in cancer KB cells

The presence of intra-nucleosome DNA fragmentation indicated apoptosis. To quantify DNA damage, the Comet assay was performed. The cells treated with the active fraction showed a substantial increase in DNA fragmentation, as evidenced by highly fragmented DNA compared to the large, non-fragmented DNA observed in the control group (Fig. 6a). Virtual images were analyzed using the CASP software to calculate various endpoints, with a particular emphasis on the DNA percentage in the comet tail, a commonly used parameter for evaluating DNA damage in the Comet assay (Fig. 6b). Remarkably, treatment with the active fraction at a concentration of 1 µg/ml consistently resulted in a significant increase in DNA percentage in the tail (35 %) and an elevation in tail movement (17 %) in KB cells.

3.11. Impact of *L. maculata* active fraction on cell cycle-related and apoptosis-related protein expressions in KB cells

The precise mechanisms by which the bioactive fraction inhibits cell growth and promotes apoptosis in KB cells were investigated in our study. Firstly, we examined cell cycle-related protein expressions, including PCNA and Cyclin D1, during cell damage. The results in Fig. 7a-b demonstrated that the active fraction significantly inhibited cell proliferation by downregulating PCNA and Cyclin D1 expression levels. This indicates that the active fraction induces cell cycle arrest, preventing the uncontrolled growth of KB cells. Additionally, we investigated apoptosis-related proteins, specifically Bax, Bcl-2, and Caspase 3, to understand the mechanisms of cell death induced by the active fraction. As shown in Fig. 7c-d, the pro-apoptotic protein Bax was significantly upregulated in KB cells treated with the active fraction, while the anti-apoptotic protein Bcl-2 was markedly downregulated. Moreover, the active fraction increased caspase-3 levels in KB cells. These findings collectively suggest that the *L. maculata* active fraction promotes apoptosis by regulating the expression of Bcl-2 family proteins and activating caspase-3, leading to cellular damage and reduced cellular proliferation. Our study reveals that the active fraction of *L. maculata* exerts its effects on KB cells by influencing both cell cycle progression and apoptosis pathways, contributing to its anticancer properties. These mechanisms provide insights into how the bioactive fraction inhibits cell growth and encourages apoptosis in KB cells.

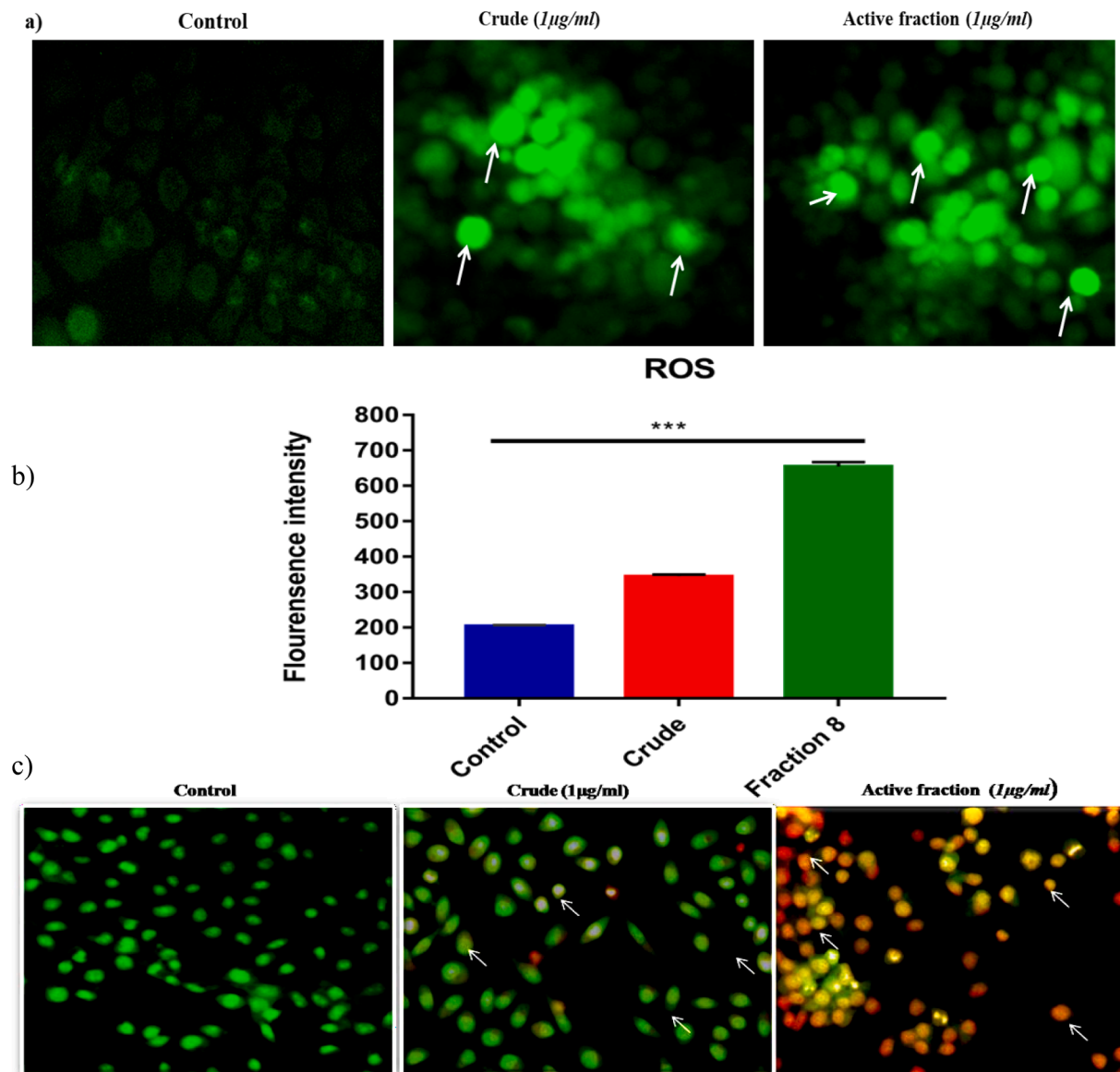


Fig. 5. Intracellular ROS levels were assessed using DCFH-DA staining fluorescence microscopy in KB cells treated with 1 µg/ml *L. maculata* active fraction, revealing a pronounced increase in DCFH fluorescence, indicating elevated intracellular ROS (a). Intracellular ROS was quantified using spectrofluorometer analysis, confirming a significant rise in ROS levels upon treatment with *L. maculata* active fraction (b). Apoptosis induction in KB cells was assessed using AO/EB staining and visualization under a fluorescence microscope (c). The active fraction-treated cells displayed distinct morphological changes and the presence of apoptotic bodies, indicating the initiation of apoptosis (20x magnification).

4. Discussion

Echinoderms, particularly starfish, are recognized for their potential medicinal properties and remarkable regenerative abilities, making them valuable models for studying regeneration at the molecular level (Schram et al., 2011). The tissue regeneration fractions of the starfish *L. maculata* were found to have a stimulating activity or to promote the wound healing processes. There is currently no clinical evidence to justify using starfish components for clinical purposes. Consequently, this study has been conducted in vitro to determine human KB cells' wound healing and anti-proliferation potential by selected starfish species. We presented the first evidence of the presence of these bioactive compounds in *L. maculata* regenerated tissue. We identified the n-butanol fraction as having potential anti-proliferative effects on KB cells and further studied its properties. Our findings align with a study by Higuchi et al., (2006), which demonstrated the biological activity of ginsenoside compounds from starfish water-soluble lipid fractions

(Higuchi et al., 2006). Similarly, previous research on *Archaster typicus* tissue extracts showed that ordinary fractions of hexane layers promote wound healing in zebrafish through in vivo and in vitro studies (Dai et al., 2016).

HPLC analysis of the active fraction revealed the presence of polar compounds that may be responsible for promoting proliferation, antioxidant activity, and cell migration in KB cells. The HPLC profile showed several peaks, with the most significant peak observed at 4.36 min, indicating the presence of active compounds. In addition to its significant impact on inhibiting KB cell growth and inducing apoptosis, the active fraction derived from *L. maculata* extracts may hold promising implications for wound healing and tissue regeneration. The GCMS/MS evaluation of the whole fractions identified 27 compounds, including amino acids, fatty acids, and organic acids. These compounds are crucial for wound healing and tissue regeneration processes. The presence of sterol-compound 5 α -Cholest-7-en-3 β -ol (Lanosterol) further supports the potential wound-healing properties of the active fraction (Kicha

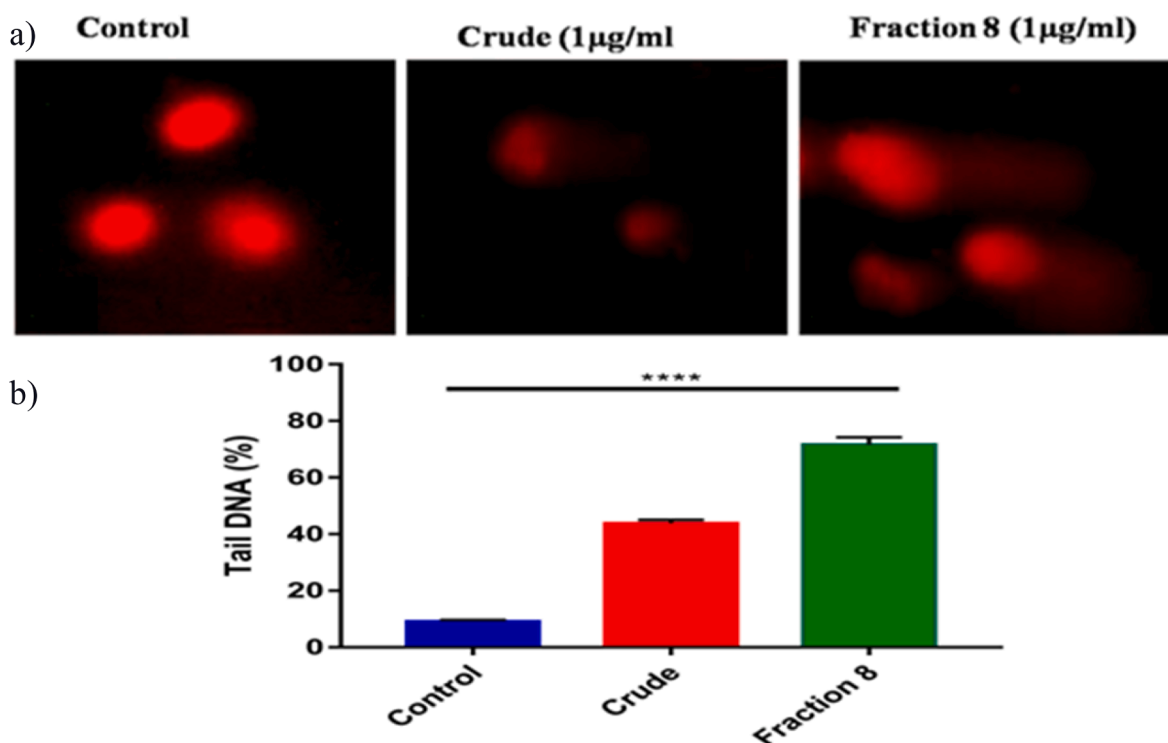


Fig. 6. Oxidative DNA damage was assessed using the comet assay, and fluorescence microscopy images of DNA fragmentation were captured in various treatment groups (a). The percentage of tail DNA, with standard deviation values from six experiments for each group was quantified as part of the comet parameter analysis (b).

et al., 2001). Furthermore, the active fraction contains essential amino acids such as glycine, proline, and arginine, present in the active fraction of *L. maculata*, play vital roles in collagen synthesis and enhancing antioxidative capacity, which is essential for effective wound healing (Wen et al., 2010). Glycine and its derivatives, such as N and N-dimethylglycine, detected through GCMS/MS analysis, are known to have detoxifying properties during wound healing. Other amino acids like arginine, cysteine, glutamine, leucine, tryptophan, and proline are essential for various metabolic pathways related to wound repair, development, and immunity (Obreshkova et al., 2012). The high glutamine content further supports the role of the active fraction in accelerating wound healing, muscle metabolism, and cellular proliferation (Pochini et al., 2014). These findings suggest that the active fraction's effects extend beyond its anticancer properties, holding promise for wound healing and tissue regeneration. However, it is important to note that further research, particularly in vivo models, is needed to explore and confirm these broader implications.

Comparatively, our study aligns with other sea cucumber species (*Holothuria scabra*, *H. fucogilya*, *H. arenicola*, *Actinopyga mauritiana*, *B. marmorata*, *H. fuscopunctata*, and *H. leucospilota*), which also exhibited increased levels of glycine and demonstrated effective wound healing (Wen et al., 2010). The active fraction's wound-healing properties are likely attributed to the hydrophobic compounds present.

In the gas chromatography study, the active fractions exhibited more polyunsaturated fatty acids (PUFAs) than saturated fatty acids. This finding is consistent with previous research, which has identified PUFAs as major essential lipids for invertebrates, regulating cell membrane fluidity and serving as precursors for animal hormones (Ridzwan et al., 2014). Our study revealed that seven out of eight compounds in the active fractions were fundamental invertebrate fatty acids, supporting the regenerative abilities of echinoderms and sea cucumbers. Notably, we observed a significant quantity of oleic acid, approximately 112.6 mg, in the active fraction. Oleic acid plays a crucial role in wound healing and tissue regeneration processes. This finding aligns with

previous studies demonstrating that applying oleic acid to wounds accelerates tissue regeneration (Pereira et al., 2008). The bioactive compounds found in *L. maculata*, especially the hydrophobic compounds, show promise as potential wound-healing agents with antioxidant and anticancer properties (Jorge et al., 2008).

In the gas chromatography study, we observed the presence of polyunsaturated fatty acids (PUFAs) rather than saturated fatty acids in the active fractions. This finding aligns with previous research where PUFAs were identified as major essential lipids for invertebrates, regulating cell membrane fluidity and serving as precursors for animal hormones (Dyall et al., 2022). Our study identified seven out of eight compounds in the active fractions as fundamental invertebrate fatty acids, consistent with the regenerative abilities of echinoderms and sea cucumbers (Pangestuti and Arifin, 2018). Specifically, we found a substantial amount of oleic acid, with 112.6 mg, in the active fraction, which plays a significant role in wound healing and tissue regeneration. This result aligns with previous studies showing that oleic acid application to wounds accelerates tissue regeneration. The bioactive compounds in *L. maculata*, particularly the hydrophobic compounds, hold promise as potential wound-healing agents with antioxidant and anticancer properties (Ambiga et al., 2007).

Our Fourier-transformed infrared (FT-IR) analysis revealed characteristic bands corresponding to amide I, II, and III in specific wavelength regions: 1653 cm⁻¹, 1454 cm⁻¹, and 1413 cm⁻¹, respectively. These bands primarily represent C = O stretching, NH bending, and C-N stretching in protein contributions (Vedantham et al., 2000). Moreover, the presence of N-H stretching and O-H free stretching and bonding was responsible for the ratio of the strong and sharp peak intensities of the bands located at wavelengths 3738.64 cm⁻¹ and 3938.64 cm⁻¹ [Table 4 in supplementary data]. These findings indicate that combining bands in the FT-IR spectra could benefit biological tissue wound-healing processes. Additionally, specific amino acid group vibrations and alkyl chain groups were detected at wavelengths 1220.94 cm⁻¹, 1112.93 cm⁻¹, and 1026.13 cm⁻¹ (Veeruraj et al., 2016). Amide III bands at 1413 cm⁻¹

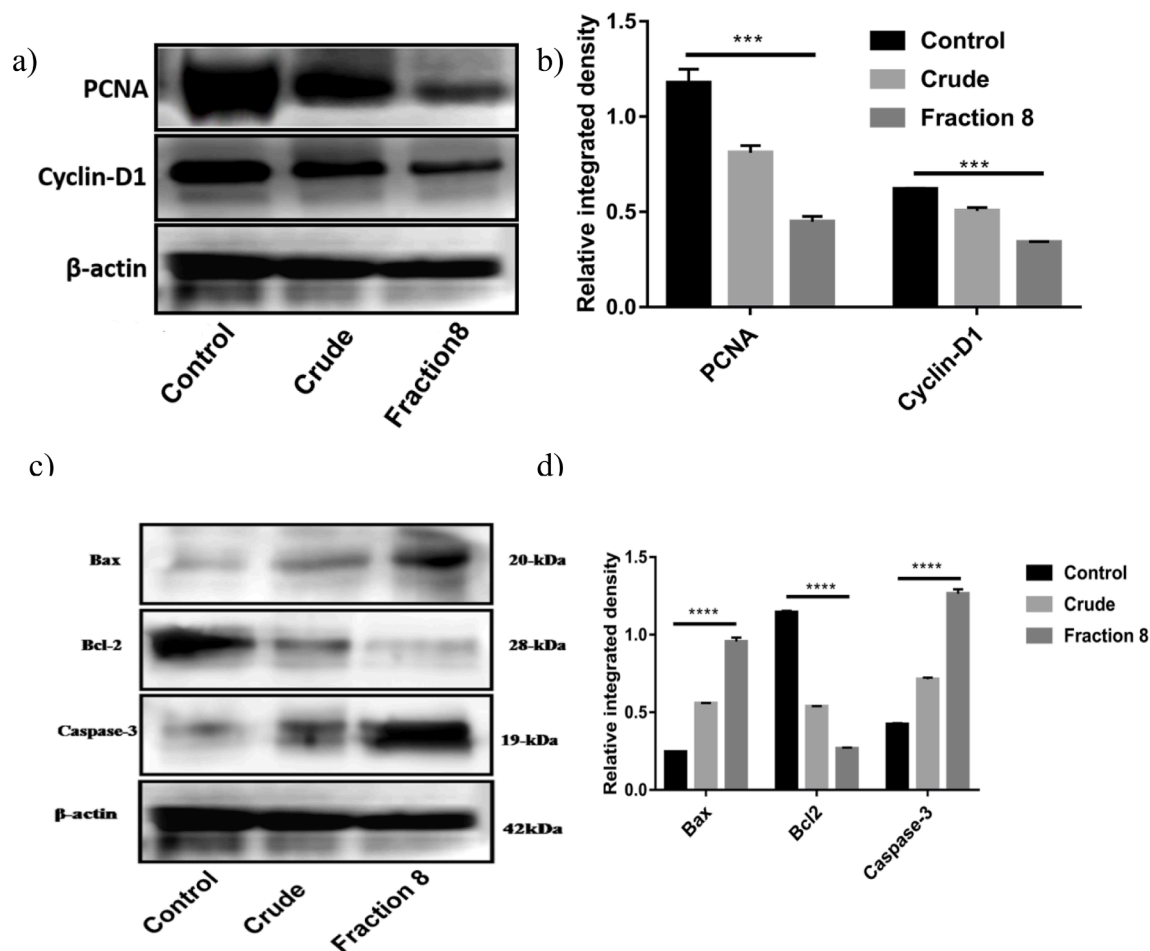


Fig. 7. Western blot analysis of PCNA and cyclin D1 (a-b) and Bcl-2, Bax, and caspase-3 (c-d) expression in control, crude, and active fraction-treated KB cells. The lysates of KB cells were subjected to immunoblotting, revealing elevated levels of Bax and caspase-3 and decreased expression of Bcl-2 in the active fraction-treated cells, suggesting the induction of apoptosis.

1 play a critical role in secondary structure determination in fish peptides (Damotharan et al., 2015). The FT-IR analysis further supports the significance of hydrophobic compounds in the active fraction for wound healing processes. Overall, the results of our study suggest that the active fraction of *L. maculata* contains bioactive compounds, such as fatty acids and proteins, which have significant potential for wound healing and tissue regeneration. These findings contribute to our understanding of the biological properties of starfish-derived compounds. They may pave the way for further research and drug discovery in wound healing.

Our study investigated the antioxidant activity of *L. maculata* extracts using the ABTS and DPPH radical scavenging assays. Free radicals cause oxidative damage to biological molecules and are associated with various health disorders, including cardiac diseases, dementia, ageing, and cancer (Suresh et al., 2010, Karthikkumar et al., 2012). The ABTS radical scavenging activity assay is commonly used to measure antioxidant activity by comparing the ability of different extracts to donate hydrogen and break free radical chains. The reduction in ABTS radical indicates the presence of antioxidants in the extracts. Similarly, the DPPH radical is widely used in biological systems to test the reducing substances, and it is sensitive enough to detect active compounds at low concentrations (Hu et al., 2011). A lower IC₅₀ value in the radical scavenging assays suggests a more efficient radical scavenging behavior. Our study demonstrated that *L. maculata* exhibits strong radical scavenging activity, as indicated by its minimum IC₅₀ value in the ABTS assay and maximum antioxidant ability in the DPPH assay.

Starfish have been found to possess antitumor cytotoxic activities

due to the presence of various compound analogues. For instance, *Culcita novaeguineae* starfish contains an asterosaponin compound that is believed to inhibit the growth of human U87MG cell and A549 lung cancer cell lines by inducing apoptosis (Zhao et al., 2011). In vitro cytotoxicity assays on *Astropectan monacanthus* showed potent activity against human promyelocytic leukemia cells (HL-60), colorectal carcinoma cells (SNU-C5), and human prostate malignancy cells (PC-3) (Thao et al., 2014). Our current study investigated the antiproliferative effects of *L. maculata* crude extracts and their active fractions on KB cell lines. Interestingly, the active fractions showed higher cell death rates than crude extracts. Inducing apoptosis in tumor cells is a crucial strategy in cancer therapies and drug development (Cheng et al., 2012). The active fraction of *L. maculata* exhibited cytotoxic activity against KB cells and induced apoptosis morphological changes in the 74 % to 78 % range at concentrations between 6.25 µg/ml and 12.5 µg/ml.

We employed fluorescence cell microscopy and observed distinct apoptotic morphology, including pyknosis, chromosomal condensation, and nuclear fission, further to investigate the mechanism of cellular death in KB cells. EtBr/AO staining revealed increased ROS levels and mitochondrial membrane damage in the KB cells treated with the active fraction. In contrast, the control cells did not show significant integration of EtBr with living cells. The present findings indicate that the active fraction of *L. maculata* induces cellular death in KB cells by increasing intracellular ROS formation and damaging their mitochondrial membranes. This is consistent with a study by Sergediene et al. (1999), which demonstrated the cytotoxic potential of *Conus vexillum* venom and its role in inducing oxidative stress.

Our study contributes valuable insights into the potential biomedical applications of *L. maculata* extracts, particularly in antioxidant activity and antitumor properties. The findings presented here shed light on the potential therapeutic applications of *L. maculata*-derived compounds and may pave the way for further research and drug discovery in the fields of antioxidant therapy and cancer treatment. Several studies have observed that active compounds derived from marine invertebrates induce apoptotic cell death through oxidative damage, leading to decreased ROS generation and loss of mitochondrial integrity in cells (Mariadoss et al., 2019b). Our study quantified ROS production using DCFH-DA on *L. maculata* active fraction. After 24 h of incubation with the active fraction, KB cells exhibited an increase in fluorescence intensity, indicating an elevated ROS level (76 % at 1 µg/ml), suggesting that the active fraction induces ROS production in KB cells, potentially leading to apoptosis morphology changes. Previous studies have reported that ROS causes apoptosis in many cancer cell lines (Jeong et al., 2010).

To further investigate the mechanism of apoptosis induction in KB cells by the active fraction, we performed DNA fragmentation assays and examined the expression of apoptosis-associated proteins. The results of this study confirmed the presence of normal morphological characteristics of apoptosis in KB cells treated with active fractions, including nuclear condensation and apoptotic formation. The comet assay also confirmed that the active fraction induces apoptosis in KB cells by causing DNA damage. Previous reports have indicated that phyto compounds can induce DNA damage in cervical cancer cells through ROS generation, which may result in increased oxidative DNA damage (Wang et al., 2008), supporting our findings that the *L. maculata* active fraction inhibits KB cell growth through the induction of apoptosis.

Our investigation into the effects of the active fraction derived from *L. maculata* on KB cells revealed several key findings that shed light on its potential mechanisms of action. Firstly, we evaluated the expression of PCNA and Cyclin D1. The treatment with the active fractions led to a notable reduction in PCNA and Cyclin D1 levels, indicative of decreased cell proliferation. In cancer cells, the deregulation of cyclin D1 is linked to regulating the G1/S cell cycle transition, making it a crucial control point in cell cycles (Arber et al., 1996). Our study suggests that the antiproliferative effects of the active fraction on KB cells are mediated by inhibiting PCNA and Cyclin D1 expression, possibly due to its antioxidant properties.

Furthermore, the expression of BCL-2 family proteins was examined to elucidate the molecular mechanisms of apoptotic induction by the active fraction in KB cells. Our results showed up-regulation of Bax and down-regulation of BCL-2, along with Caspase 3 activation, which is all associated with apoptosis in KB cells induced by the active fraction (Ren et al., 2008). Sequential caspase activation plays a significant role in implementing cell apoptosis. (Heo et al., 2011). Overall, our findings suggest that the active fraction of *L. maculata* may inhibit KB cell proliferation through mechanisms related to apoptosis induction, involving the regulation of BCL-2 family proteins and caspase activation. While our study did not directly investigate the tissue regeneration mechanisms in *L. maculata* starfish, the observed effects on KB cells provide intriguing insights into the potential interplay between tissue regeneration and anticancer properties. Further research, including studies on tissue regeneration pathways in starfish, may help elucidate the broader implications of our findings. We believe exploring these potential connections could open new avenues for cancer therapy and regenerative medicine.

In addition to elucidating apoptosis induction mechanisms, it's vital to address previous limitations in crude *L. maculata* extract studies. These limitations often involve compound identification and specificity, with many failings to pinpoint bioactive compounds. Our research overcomes these issues using advanced techniques like NMR spectroscopy, HR-MS, and MS/MS for precise compound identification. This enables us to associate specific compounds with observed biological activities. Furthermore, our study focuses on key mechanisms, such as

apoptosis and antioxidant activity, enhancing our understanding of *L. maculata* extract potential in cancer therapy.

5. Conclusions

In conclusion, our in vitro study on the regenerative tissues of *L. maculata* starfish demonstrated the bioactive fraction's inhibitory effect on proliferation, induction of apoptosis, and increased ROS levels, leading to oxidative DNA damage. Identifying biomaterial compounds through HPLC and GC-MS/MS provided valuable insights into the presence of fatty acids, amino acids, alcohols, sterols, carbohydrates, and hydrocarbons. Notably, 5-Cholest-7-en-3β-ol, a sterol, was among the identified fatty acids. Several bioactive components, such as Hexadecanoic acid, Myo-Inositol, 9, 12, 15-Octadecatrienoic acid, and 9,12-Octadecadienoic acid, were confirmed to possess antioxidant and anticancer properties. This study represents the first documentation of the composition of regenerative tissues in *L. maculata*. It highlights its bioactive compounds, revealing its potential as an agent with anti-proliferative, antioxidant, and apoptotic induction properties. Further research on these starfish animal models may provide sufficient evidence to support their potential as drugs for various types of cancer.

Author contributions

PN, LRPL has designed and done the experimental study and wrote the original manuscript; ASS, CG, RK, KR, MS, CCS, also helped design the study, analyzed the data and supervised the experiments, reviewed, and edited the manuscript. AYG has contributed to the data interpretation and discussion. All authors have read and proofread the manuscript.

Funding

This project was supported by Researchers Supporting Project number (RSPD2023R712), King Saud University, Riyadh, Saudi Arabia.

Declaration of competing interest

The authors declare that they have no known competing financial interests or personal relationships that could have appeared to influence the work reported in this paper.

Acknowledgments

The authors are thankful to Aarupadai Veedu Medical College, Vinayaka Mission's Research Foundation (Deemed to be University), Kirumampakkam, Puducherry- 607402, India for the support provided.

Appendix A. Supplementary material

Supplementary data to this article can be found online at <https://doi.org/10.1016/j.jksus.2023.103035>.

References

- Al-Assaf, S., Phillips, G.O., Aoki, H., et al., 2007. Characterization and properties of *Acacia senegal* (L.) Willd. var. *senegal* with enhanced properties (*Acacia* (sen) SUPER GUM™): Part 1—Controlled maturation of *Acacia senegal* var. *senegal* to increase viscoelasticity, produce a hydrogel form and convert a poor into a good emulsifier. *Food Hydrocoll.* 21 (3), 319–328.
- Ambiga, S., Narayanan, R., Gowri, D., et al., 2007. Evaluation of wound healing activity of flavonoids from *Ipomoea Carnea* Jacq. *Anc. Sci. Life* 26 (3), 45–51.
- Arber, N., Hibshoosh, H., Moss, S.F., et al., 1996. Increased expression of cyclin D1 is an early event in multistage colorectal carcinogenesis. *Gastroenterology* 110 (3), 669–674. <https://doi.org/10.1053/gast.1996.v110.pm8608874>.
- Baker, D.H., Han, Y., 1994. Ideal amino acid profile for chicks during the first three weeks posthatching. *Poult. Sci.* 73 (9), 1441–1447.
- Balamurugan, M., Sivakumar, K., Mariadoss, A.V., et al., 2017. Modulating effect of *Hypnea musciformis* (Red Seaweed) on lipid peroxidation, antioxidants and

- biotransforming enzymes in 7,12-dimethylbenz (a) anthracene induced mammary carcinogenesis in experimental animals. *Pharmacogn. Res.* 9 (1), 108–115. <https://doi.org/10.4103/0974-8490.187085>.
- Ben Khadra, Y., M. Sugni, C. Ferrario, et al., 2018. Regeneration in Stellate Echinoderms: Crinoidea, Asteroidea and Ophiuroidea. *Marine Organisms as Model Systems in Biology and Medicine*. M. Kloc and J. Z. Kubiak. Cham, Springer International Publishing: 285–320.
- Bligh, E.G., Dyer, W.J., 1959. A rapid method of total lipid extraction and purification. *Can. J. Biochem. Physiol.* 37 (8), 911–917.
- Cheng, X., Xiao, Y., Wang, X., et al., 2012. Anti-tumor and pro-apoptotic activity of ethanolic extract and its various fractions from *Polytrichum commune* L. ex Hedw in L1210 cells. *J. Ethnopharmacol.* 143 (1), 49–56. <https://doi.org/10.1016/j.jep.2012.05.054>.
- Dai, Y., Prithiviraj, N., Gan, J., et al., 2016. Tissue extract fractions from starfish undergoing regeneration promote wound healing and lower jaw blastema regeneration of zebrafish. *Sci. Rep.* 6 (1), 38693.
- Damotharan, P., Veeruraj, A., Arumugam, M., et al., 2015. Isolation and characterization of biologically active venom protein from sea snake *Enhydrina schistosa*. *J. Biochem. Mol. Toxicol.* 29 (3), 140–147. <https://doi.org/10.1002/jbt.21678>.
- Dong, G., Xu, T., Yang, B., et al., 2011. Chemical constituents and bioactivities of starfish. *Chem. Biodivers.* 8 (5), 740–791. <https://doi.org/10.1002/cbdv.200900344>.
- Duke, J. and M. J. Bogenschutz, 1994. *Dr. Duke's phytochemical and ethnobotanical databases*, USDA, Agricultural Research Service Washington, DC.
- Dyall, S.C., Balas, L., Bazan, N.G., et al., 2022. Polyunsaturated fatty acids and fatty acid-derived lipid mediators: Recent advances in the understanding of their biosynthesis, structures, and functions. *Prog. Lipid Res.* 86, 101165 <https://doi.org/10.1016/j.plipres.2022.101165>.
- García-Ararrás, J.E., Dolmatov, I.Y., 2010. Echinoderms: potential model systems for studies on muscle regeneration. *Curr. Pharm. Des.* 16 (8), 942–955. <https://doi.org/10.2174/138161210790883426>.
- Gülçin, I., Küfrevioğlu, O.I., Oktay, M., et al., 2004. Antioxidant, antimicrobial, antitumor and analgesic activities of nettle (*Urtica dioica* L.). *J. Ethnopharmacol.* 90 (2–3), 205–215. <https://doi.org/10.1016/j.jep.2003.09.028>.
- Gunaseelan, S., Balupillai, A., Govindasamy, K., et al., 2017. Linalool prevents oxidative stress activated protein kinases in single UVB-exposed human skin cells. *PLoS One* 12 (5), e0176699. <https://doi.org/10.1371/journal.pone.0176699>.
- Heo, S.J., Kim, K.N., Yoon, W.J., et al., 2011. Chromene induces apoptosis via caspase-3 activation in human leukemia HL-60 cells. *Food Chem. Toxicol. : Int. J. Published Br. Indus. Biol. Res. Assoc.* 49 (9), 1998–2004. <https://doi.org/10.1016/j.fct.2011.05.011>.
- Higuchi, R., Inoue, S., Inagaki, K., et al., 2006. Biologically active glycosides from asteroidea, 42. Isolation and structure of a new biologically active ganglioside molecular species from the starfish *Asterina pectinifera*. *Chem. Pharm. Bull.* 54 (3), 287–291.
- Hu, W., Yu, L., Wang, M.H., 2011. Antioxidant and antiproliferative properties of water extract from *Mahonia bealei* (Fort.) Carr. leaves. *Food Chem. Toxicol.* 49 (4), 799–806. <https://doi.org/10.1016/j.fct.2010.12.001>.
- Ilyasov, I.R., Beloborodov, V.L., Selivanova, I.A., et al., 2020. ABTS/PP decolorization assay of antioxidant capacity reaction pathways. *Int. J. Mol. Sci.* 21 (3), 1131.
- Jeong, J.C., Jang, S.W., Kim, T.H., et al., 2010. Mulberry fruit (*Morus fructus*) extracts induce human glioma cell death in vitro through ROS-dependent mitochondrial pathway and inhibits glioma tumor growth in vivo. *Nutr. Cancer* 62 (3), 402–412. <https://doi.org/10.1080/01635580903441287>.
- Jorge, M.P., Madjarof, C., Gois Ruiz, A.L., et al., 2008. Evaluation of wound healing properties of *Arrabidaea chica* Verlot extract. *J. Ethnopharmacol.* 118 (3), 361–366. <https://doi.org/10.1016/j.jep.2008.04.024>.
- Karthikumar, V., Sivagami, G., Vinothkumar, R., et al., 2012. Modulatory efficacy of rosmarinic acid on premalignant lesions and antioxidant status in 1,2-dimethylhydrazine induced rat colon carcinogenesis. *Environ. Toxicol. Pharmacol.* 34 (3), 949–958. <https://doi.org/10.1016/j.etap.2012.07.014>.
- Kicha, A.A., Ivanchina, N.V., Gorshkova, I.A., et al., 2001. The distribution of free sterols, polyhydroxysteroids and steroid glycosides in various body components of the starfish *Patiria (= Asterina) pectinifera*. *Comp. Biochem. Physiol. B Biochem. Mol. Biol.* 128 (1), 43–52.
- Krimm, S., Bandekar, J., 1986. Vibrational spectroscopy and conformation of peptides, polypeptides, and proteins. *Adv. Protein Chem.* 38, 181–364.
- Mann, J., 2002. Natural products in cancer chemotherapy: past, present and future. *Nat. Rev. Cancer* 2 (2), 143–148.
- Mariadoss, A. V. A., S. Park, K. Saravankumar, et al., 2021. Ethyl Acetate Fraction of *Helianthus tuberosus* L. Induces Anti-Diabetic, and Wound-Healing Activities in Insulin-Resistant Human Liver Cancer and Mouse Fibroblast Cells. *Antioxidants* (Basel, Switzerland). 10 (1) <https://doi.org/10.3390/antiox10010099>.
- Mariadoss, A.V.A., Ramachandran, V., Shalini, V., et al., 2019a. Green synthesis, characterization and antibacterial activity of silver nanoparticles by *Malus domestica* and its cytotoxic effect on (MCF-7) cell line. *Microb. Pathog.* 135, 103609 <https://doi.org/10.1016/j.micpath.2019.103609>.
- Mariadoss, A.V.A., Vinayagam, R., Senthilkumar, V., et al., 2019b. Phloretin loaded chitosan nanoparticles augments the pH-dependent mitochondrial-mediated intrinsic apoptosis in human oral cancer cells. *Int. J. Biol. Macromol.* 130, 997–1008. <https://doi.org/10.1016/j.ijbiomac.2019.03.031>.
- Meyer-Rochow, V.B., 2017. Therapeutic arthropods and other, largely terrestrial, folk-medicinally important invertebrates: a comparative survey and review. *J. Ethnobiol. Ethnomed.* 13 (1), 1–31.
- Obreshkova, D.P., Tsvetkova, D.D., Ivanov, K.V., 2012. Simultaneous identification and determination of total content of aminoacids in food supplements-tablets by gas chromatography. *Asian J. Pharm. Clin. Res.* 5 (2), 57–68.
- Pangestuti, R., Arifin, Z., 2018. Medicinal and health benefit effects of functional sea cucumbers. *J. Tradit. Complement. Med.* 8 (3), 341–351. <https://doi.org/10.1016/j.jtcme.2017.06.007>.
- Pereira, L.M., Hatanaka, E., Martins, E.F., et al., 2008. Effect of oleic and linoleic acids on the inflammatory phase of wound healing in rats. *Cell Biochem. Funct.: Cell. Biochem. Modul. Active Agents Dis.* 26 (2), 197–204.
- Pochini, L., Scalise, M., Galluccio, M., et al., 2014. Membrane transporters for the special amino acid glutamine: structure/function relationships and relevance to human health. *Front. Chem.* 2, 61.
- Qingming, Y., Xianhui, P., Weibao, K., et al., 2010. Antioxidant activities of malt extract from barley (*Hordeum vulgare* L.) toward various oxidative stress in vitro and in vivo. *Food Chem.* 118 (1), 84–89.
- Ren, G., Zhao, Y.P., Yang, L., et al., 2008. Anti-proliferative effect of clitocine from the mushroom *Leucopaxillus giganteus* on human cervical cancer HeLa cells by inducing apoptosis. *Cancer Lett.* 262 (2), 190–200. <https://doi.org/10.1016/j.canlet.2007.12.013>.
- Ridzwan, B.H., Hanita, M.H., Nurzafira, M., et al., 2014. Free fatty acids composition in lipid extracts of several sea cucumbers species from Malaysia. *Int. J. Biosci. Biochem. Bioinform.* 4 (3), 204.
- Schram, J.B., McClintock, J.B., Angus, R.A., et al., 2011. Regenerative capacity and biochemical composition of the sea star *Luidia clathrata* (Say) (Echinodermata: Asteroidea) under conditions of near-future ocean acidification. *J. Exp. Mar. Biol. Ecol.* 407 (2), 266–274.
- Sergedine, E., Jönsson, K., Szymysiak, H., et al., 1999. Prooxidant toxicity of polyphenolic antioxidants to HL-60 cells: description of quantitative structure-activity relationships. *FEBS Lett.* 462 (3), 392–396. [https://doi.org/10.1016/S0014-5793\(99\)01561-6](https://doi.org/10.1016/S0014-5793(99)01561-6).
- Sivaraj, M., Mukherjee, A., Mariappan, R., et al., 2018. Polyorganophosphazene stabilized gold nanoparticles for intracellular drug delivery in breast carcinoma cells. *Process Biochem.* 72, 152–161.
- Suresh, K., Manoharan, S., Vijayaananand, M.A., et al., 2010. Chemopreventive and antioxidant efficacy of (6)-paradol in 7,12-dimethylbenz(a)anthracene induced hamster buccal pouch carcinogenesis. *Pharmacol. Rep.* 62 (6), 1178–1185. [https://doi.org/10.1016/S1734-1140\(10\)70380-7](https://doi.org/10.1016/S1734-1140(10)70380-7).
- Thao, N.P., Luyen, B.T., Kim, E.J., et al., 2014. Asteroaponins from the Starfish *Astropecten monacanthus* suppress growth and induce apoptosis in HL-60, PC-3, and SNU-C5 human cancer cell lines. *Biol. Pharm. Bull.* 37 (2), 315–321. <https://doi.org/10.1248/bpb.b13-00705>.
- Vedantham, G., Sparks, H.G., Sane, S.U., et al., 2000. A holistic approach for protein secondary structure estimation from infrared spectra in H(2)O solutions. *Anal. Biochem.* 285 (1), 33–49. <https://doi.org/10.1006/abio.2000.4744>.
- Veeruraj, A., Pugazhvendan, S.R., Ajithkumar, T.T., et al., 2016. Isolation and identification of cytotoxic and biological active toxin from the puffer fish *Arothron stellatus*. *Toxicol. Res.* 32 (3), 215–223. <https://doi.org/10.5487/tr.2016.32.3.215>.
- Venkatachalam, K., Vnayakam, S., Sahathevan, K., et al., 2018. Thymol enhances antioxidant defense and inhibits Lipid Peroxidation in 1, 2-dimethylhydrazine-induced Colon cancer. *KMJ-Kuwait Med. J.* 50 (4), 447–454.
- Veríssimo, A.C.S., Pacheco, M., Silva, A.M.S., et al., 2021. Secondary metabolites from marine sources with potential use as leads for anticancer applications. *Molecules* 26 (14). <https://doi.org/10.3390/molecules26144292>.
- Wang, T., Chen, L.X., Long, Y., et al., 2008. DNA damage induced by caffeic acid phenyl ester in the presence of Cu(II) ions: potential mechanism of its anticancer properties. *Cancer Lett.* 263 (1), 77–88. <https://doi.org/10.1016/j.canlet.2007.12.021>.
- Wen, J., Hu, C., Fan, S., 2010. Chemical composition and nutritional quality of sea cucumbers. *J. Sci. Food Agric.* 90 (14), 2469–2474.
- Zhao, Y., Zhu, C., Li, X., et al., 2011. Asteroaponin 1 induces endoplasmic reticulum stress-associated apoptosis in A549 human lung cancer cells. *Oncol. Rep.* 26 (4), 919–924. <https://doi.org/10.3892/or.2011.1358>.
- Zhu, K.-X., Lian, C.-X., Guo, X.-N., et al., 2011. Antioxidant activities and total phenolic contents of various extracts from defatted wheat germ. *Food Chem.* 126 (3), 1122–1126. <https://doi.org/10.1016/j.foodchem.2010.11.144>.
- Zhu, K., Zhou, H., Qian, H., 2006. Antioxidant and free radical-scavenging activities of wheat germ protein hydrolysates (WGPH) prepared with alcalase. *Process Biochem.* 41 (6), 1296–1302.